

THERMAL X-RAYS FROM MILLISECOND PULSARS: CONSTRAINING THE FUNDAMENTAL PROPERTIES OF NEUTRON STARS

SLAVKO BOGDANOV, JONATHAN E. GRINDLAY, AND GEORGE B. RYBICKI

Harvard-Smithsonian Center for Astrophysics, 60 Garden Street, Cambridge, MA 02138;

sbogdanov@cfa.harvard.edu, josh@cfa.harvard.edu

Received 2007 August 21; accepted 2008 August 1

ABSTRACT

We model the X-ray properties of millisecond pulsars (MSPs) by considering hot-spot emission from a weakly magnetized neutron star (NS) covered by a hydrogen atmosphere. We investigate the limitations of using the thermal X-ray pulse profiles of MSPs to constrain the mass-to-radius (M/R) ratio of the NS. The accuracy is strongly dependent on the viewing angle and magnetic inclination, but is ultimately limited only by photon statistics. We demonstrate that valuable information regarding NSs can be extracted, even from data of fairly limited photon statistics through modeling of archival observations of the nearby isolated PSRs J0030+0451 and J2124–3358. The X-ray emission from these pulsars is consistent with the presence of an atmosphere and a dipolar field configuration. For both MSPs, the favorable geometry allows us to place limits on the allowed M/R of NSs. Assuming $1.4 M_{\odot}$, the stellar radius is constrained to be $R > 9.4$ km and $R > 7.8$ km (68% confidence) for PSRs J0030+0451 and J2124–3358, respectively. We explore the prospects of using future observatories such as *Constellation-X* and *XEUS* to conduct X-ray–timing searches for MSPs not detectable at radio wavelengths due to unfavorable viewing geometry. We are also able to place strong constraints on the magnetic field evolution model proposed by Ruderman. The pulse profiles indicate that the magnetic field of an MSP does not have a tendency to align itself with the spin axis or migrate toward one of the spin poles during the low-mass X-ray binary phase.

Subject headings: pulsars: general — pulsars: individual (PSR J0030+0451, PSR J2124–3358) — stars: neutron — X-rays: stars

Online material: color figures

1. INTRODUCTION

Recent X-ray studies have revealed that a number of known rotation-powered millisecond pulsars (MSPs) exhibit predominantly thermal soft X-ray emission (Grindlay et al. 2002; Zavlin 2006, 2007; Bogdanov et al. 2006a). The inferred effective emission radii R_{eff} indicate that this radiation is localized in regions on the neutron star (NS) surface much smaller than the expected stellar radius ($R_{\text{eff}} \ll R$), but comparable to the classical radius of the pulsar magnetic polar cap $R_{\text{pc}} = (2\pi R/cP)^{1/2} R$. This finding agrees with theoretical models of pulsars, which indicate that the conditions in the magnetosphere of a typical MSP favor heating of the polar caps to $\sim 10^6$ K by a return flow of energetic particles along the open magnetic field lines (see, e.g., Harding & Muslimov 2002; Zhang & Cheng 2003 for details). As this heat is restricted to a small fraction of the NS, studying the X-ray spectra and pulse profiles of MSPs can reveal important information about the star, such as the radiative properties of the NS surface, magnetic field geometry, and NS compactness (R/R_s , where $R_s = 2GM/c^2$). This approach, originally proposed by Pavlov & Zavlin (1997) in the context of radio MSPs, can serve as a valuable probe of key NS properties that are inaccessible by other observational means (e.g., radio pulse timing). As shown by Pavlov & Zavlin (1997), Zavlin & Pavlov (1998), and Bogdanov et al. (2007), a model of polar cap thermal emission from an optically thick hydrogen (H) atmosphere provides an excellent description of the X-ray pulse profiles of PSR J0437–4715, the nearest known MSP. On the other hand, a blackbody model is inconsistent with the X-ray–timing data and can be definitively ruled out. Furthermore, there is compelling evidence for a magnetic dipole axis offset from the NS center (Bogdanov et al. 2007). Finally, the compactness of PSR J0437–4715 is constrained to

be $R/R_s > 1.6$ (99.9% confidence). Thus, modeling of X-ray data of MSPs appears to be a very promising approach toward answering long-standing questions regarding the fundamental properties of MSPs and NSs in general.

The present paper represents an extension of the work described in Bogdanov et al. (2007). Here we explore the detailed properties of the MSP X-ray emission model with particular emphasis on its use for constraints on the NS equation of state (EOS). The work is organized as follows. In § 2 we examine the properties of our model; in § 3 we discuss an application of our model to archival X-ray observations of PSRs J0030+0451 and J2124–3358. In § 4 we present a discussion and end with conclusions in § 5.

2. MODEL ANALYSIS

The specifics of the theoretical model employed in this work are outlined in Bogdanov et al. (2007). In brief, the model considers a relativistic rotating compact star with two identical X-ray–emitting hot spots, which in the case of MSPs (presumably) correspond to the magnetic polar caps. The position of each spot relative to the observer is given by the angle ψ defined as

$$\cos \psi(t) = \sin \alpha \sin \zeta \cos \phi(t) + \cos \alpha \cos \zeta, \quad (1)$$

where α is the pulsar obliquity (i.e., angle between the spin and magnetic axes), ζ is the angle between the pulsar spin axis and the line of sight to the distant observer, and $\phi(t)$ is the spin phase. We take a nonrotating Schwarzschild metric as a description of the space-time in the vicinity of the NS and include Doppler boosting and propagation time delays. This formalism is remarkably accurate, as long as the spin period of the star is $\gtrsim 3$ ms,

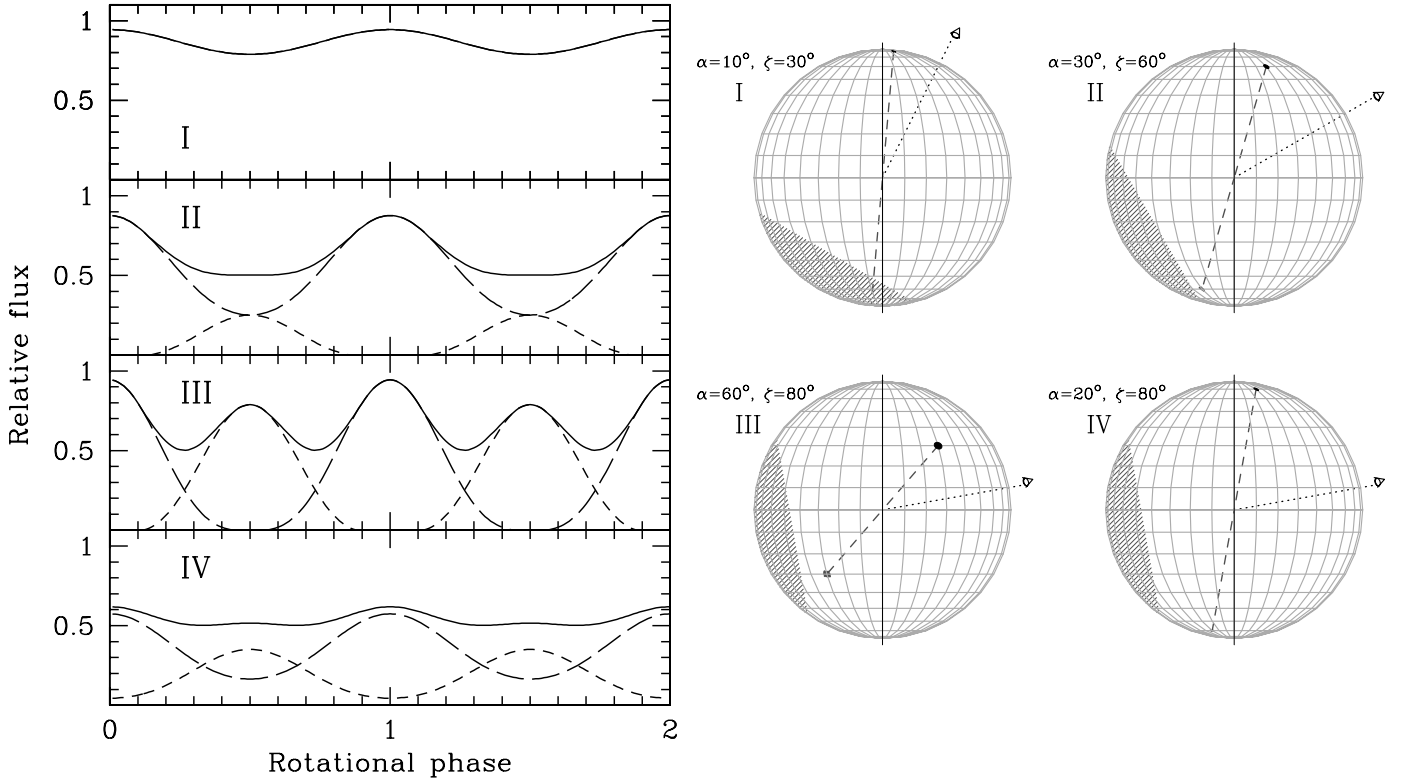


FIG. 1.—*Left*: Representative synthetic hydrogen atmosphere light curves for a rotating $M = 1.4 M_{\odot}$, $R = 10$ km NS with two antipodal hot spots for the four light-curve classes (I–IV, from top to bottom, respectively) defined by Beloborodov (2002). The dashed lines show the individual flux contribution from the two hot spots, while the solid line shows the total observed flux. All fluxes are normalized to the value corresponding to a face-on hot spot ($\alpha = \zeta = 0$). Two rotational cycles are shown for clarity. *Right*: Orthographic map projection of the MSP surface for the four pulse profiles. The dashed line shows the magnetic axis, while the dotted line shows the line of sight to the observer. The hatched region corresponds to the portion of the star not visible to the observer.

where rotation-induced oblateness is unimportant (Cadeau et al. 2007). The NS surface is assumed to be covered by an unmagnetized ($B < 10^9$ G), optically thick H atmosphere (Zavlin et al. 1996; McClintock et al. 2004). The angle-dependent emission pattern of this atmosphere differs substantially from the isotropic one of a blackbody, which is particularly evident in the rotation-induced modulations of the X-ray flux (see Fig. 1 of Bogdanov et al. 2007).

Using this model, we generate both synthetic spectra and pulse profiles (Fig. 1) for the following parameters: the effective temperatures and radii of the emission region(s) T_1 , T_2 , R_1 and R_2 , α , ζ , and M/R . Unless noted otherwise, we fix the mass to the canonical NS value $M = 1.4 M_{\odot}$ and vary only R . We also allow for an off-center magnetic axis by including offsets in the position of the secondary hot spot in latitude and longitude, $\Delta\alpha$ and $\Delta\phi$, respectively, from the antipodal position. The corresponding net offset of the secondary hot spot from the antipodal position across the NS surface is¹

$$\Delta s = R \cos^{-1} [\cos \alpha \cos (\alpha + \Delta\alpha) + \sin \alpha \sin (\alpha + \Delta\alpha) \cos \Delta\phi], \quad (2)$$

while the total displacement (i.e., impact parameter) of the magnetic axis from the stellar center is

$$\Delta x = R \sin \left(\frac{\Delta s}{2R} \right). \quad (3)$$

¹ Note that eq. (12) in Bogdanov et al. (2007) is valid only if the angle α is reckoned from the equator toward the spin pole. However, as defined by convention, the pulsar obliquity α is measured from the spin pole toward the equator. Thus, the correct expression for the secondary hot spot offset is given by eq. (2) in this present paper.

We conduct fits to both the spectrum and pulse profile. As pointed out by Pavlov & Zavlin (1997), this is important because the spectral fits provide tight constraints on T_{eff} and R_{eff} , but do not provide useful information regarding the system geometry or M/R . Conversely, the pulse profiles provide constraints on the compactness and geometry of the NS, but are less sensitive to the parameters that define the emission spectrum (T_{eff} and R_{eff}).

2.1. Extended versus Pointlike Emission

In Bogdanov et al. (2007), only pointlike hot spots were considered, which was sufficient for application to the available data for J0437–4715. Here we also consider more realistic extended hot spots in order to ascertain the effect of the uncertain physical size and shape of the hot polar caps on the observed pulse profiles. To accomplish this, we consider a grid of emission spots across the NS surface, which allows us to construct X-ray emission regions of arbitrary size and shape. Figure 2 shows the resulting pulse profiles for two extreme cases, (1) a uniformly heated, circular polar cap of radius 2 km and (2) a thin annulus (with thickness much smaller than its radius), also with a 2 km radius. The value $R_{\text{pc}} = 2$ km corresponds to the expected polar cap radius of a $P = 5$ ms pulsar. Surprisingly, the physical extent and exact shape of the emission regions do not significantly affect the observed pulse profile and differ from the pointlike case by only $\lesssim 1\%$, except for class IV, for which they differ by as much as $\sim 15\%$. The largest differences occur at the turning points of the light curves.

In reality, due to the rotation of the pulsar the polar cap shape is probably distorted (see, e.g., Narayan & Vivekanand 1983; Biggs 1990), with elongation or compression in the meridional (north-south) direction on the NS surface. However, even in such

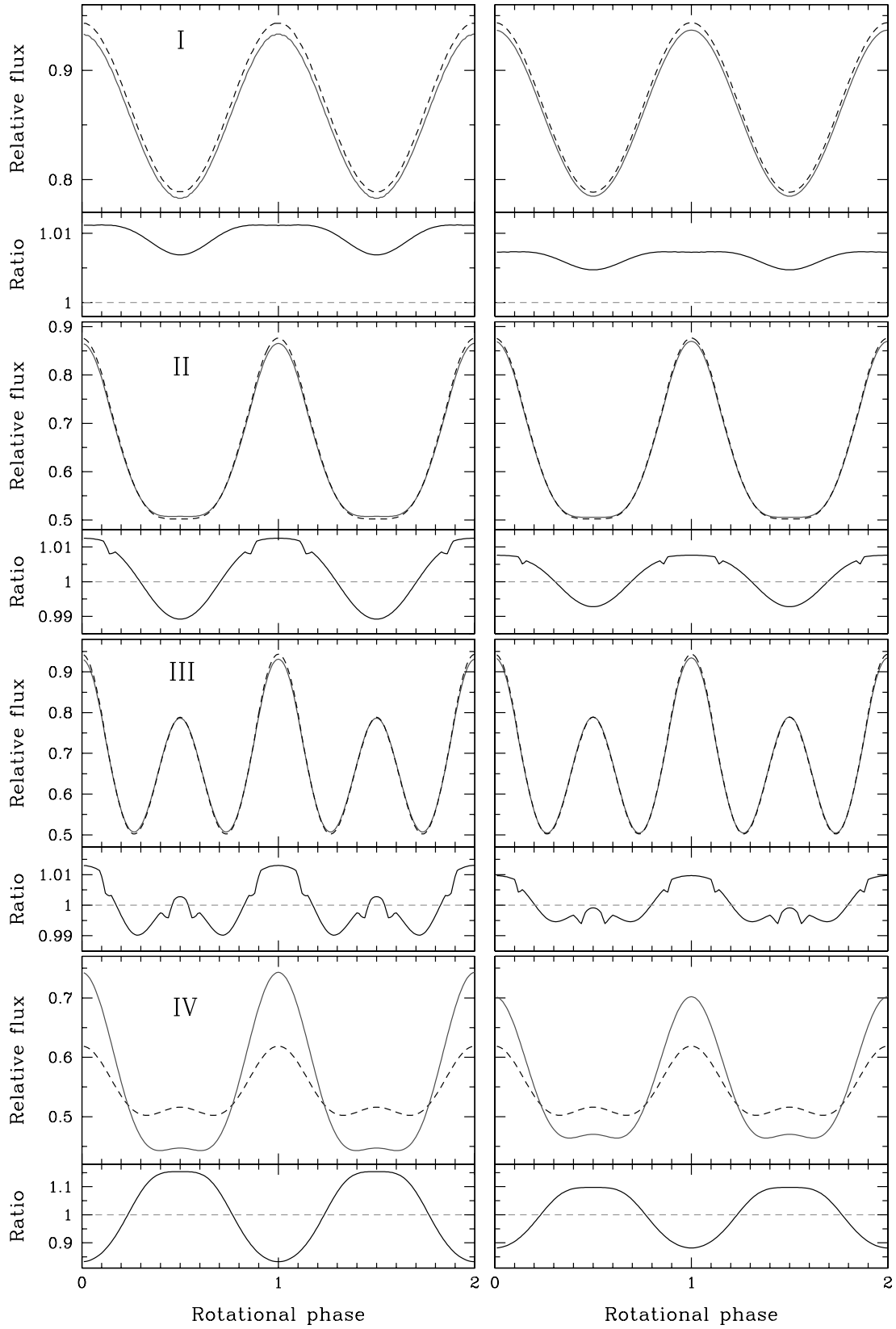


FIG. 2.—Light curves for a rotating $M = 1.4 M_{\odot}$, $R = 10$ km NS with two antipodal hot spots with values of α and ζ as in Fig. 1. The dashed line shows the idealized case of pointlike hot spots, while the solid line is for the case of a filled circular hot spot (*left set of plots*) and a thin annulus (*right set of plots*), both of radius 2 km and $T_{\text{eff}} = 2 \times 10^6$ K. The bottom panel for each class shows the ratio between the two light curves shown in the top panel. All fluxes are normalized to the value corresponding to $\alpha = \zeta = 0$. Two rotational cycles are shown for clarity. [See the electronic edition of the *Journal* for a color version of this figure.]

instances the differences from a circular hot spot with the same effective area are relatively small (a few %). This also means that for emission regions on the NS surface comparable in area to that expected for a circular pulsar polar cap, the X-ray pulse profiles do not provide useful information regarding the details of the region geometry. Moreover, the weak dependence of the pulse profile on the polar cap size implies that the distance to the pulsar, which is covariant with the emission area through the flux normalization (R_{eff}^2/D^2), does not significantly affect the pulse profile shape and pulsed fraction. Thus, unlike alternative methods for measuring NS compactness (e.g., using quiescent low-mass X-ray binaries [LMXBs]), fits to the X-ray pulse profiles of MSPs are not strongly affected by uncertainties in the distance. Finally, Figure 2 implies that the pulse profiles are weakly sensitive to broadband calibration uncertainties in the detector effective area as well. Narrowband deviations from the true effective area of the instrument (for instance, near absorption edges) are also negligible, as the pulse profiles cover relatively wide energy intervals (see § 2.2).

Note that the ambiguity in the exact shape of the polar caps may ultimately limit the accuracy of the constraint on the desirable NS parameters using the approach described here. Nonetheless, for the observed spectra of MSPs (see, e.g., Zavlin 2006), the effective radius of the hotter emission region is found to be of order a few hundred meters, which compared to the size of the star (~ 10 km) is effectively pointlike. Thus, the uncertainty in the true shape of the emission region can be overcome by considering only the hotter emission component.

2.2. Limiting Accuracy of M/R Constraints Using MSPs

It has been shown that combined X-ray spectroscopic and timing studies of rotation-powered MSPs can be used to infer the M/R of the NS (Pavlov & Zavlin 1997; Zavlin & Pavlov 1998; Bogdanov et al. 2007). Here we wish to determine whether with further improvement in data quality, M/R can be determined to significantly better accuracy. This is essential if this method is to be used for reliable measurements of the NS compactness and ultimately the NS EOS. In addition, it is important to ascertain how the viewing and magnetic geometries affect the constraints on the desired NS parameters. For this purpose, we have carried out a series of fits to simulated X-ray data of MSPs with greatly improved photon statistics compared to those currently available. A major advantage of the greatly increased data quality is the possibility of high signal-to-noise ratio energy-resolved pulse profiles in multiple energy bands and phase-resolved spectroscopy for several phase windows. As an illustration, we consider the current version of the proposed effective area curve of the *Constellation-X* observatory X-Ray Microcalorimeter Spectrometer (XMS) detector² and assume a range of exposure times, spanning from 250 ks to 1 Ms. We generate representative light curves for each of the four distinct types defined by Beloborodov (2002) based on the visibility of the two antipodal hot spots (see Figs. 1 and 3), assuming both $R = 10$ km and $M = 1.4 M_{\odot}$, representative of strange equations of state, and $R = 12$ and $M = 1.4$, expected from conventional nucleonic equations of state (Lattimer & Prakash 2001).

Class I pulse profiles occur in cases when only the primary hot spot is observable at all times, while the secondary hot spot is in the invisible portion of the star for the entire period (see Fig. 1). Note that for two antipodal polar caps, this can be achieved only

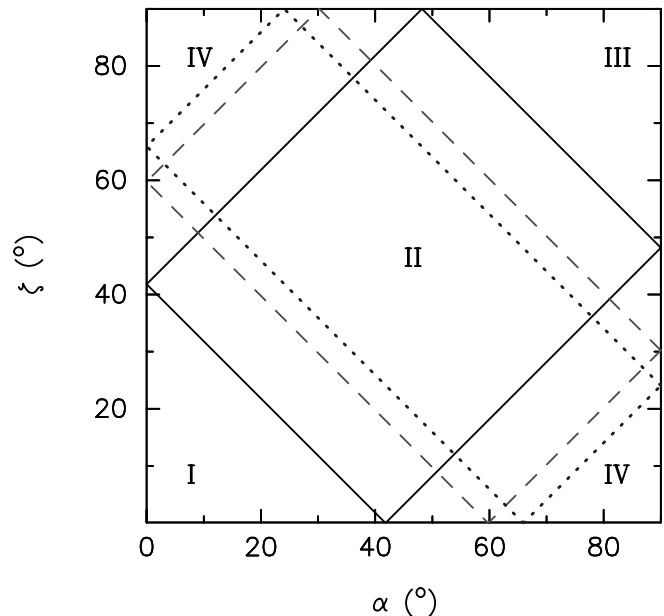


FIG. 3.—Location of pulse profile classes I–IV on the α - ζ plane for MSPs with $R = 10$ (solid line), 12 (dashed line), and 14 (dotted line) km, assuming $M = 1.4 M_{\odot}$. See Fig. 1 and text for a definition of each class. [See the electronic edition of the *Journal* for a color version of this figure.]

for $R/R_s > 1.7$ (or $R > 7$ km for $M = 1.4 M_{\odot}$), since for a more compact star the entire stellar surface is always visible. The visibility of only a single hot spot causes large uncertainties regarding the true geometry and especially the compactness. This occurs because that visible hot spot is always found at a small angle with respect to the line of sight, where light-bending effects are less pronounced, resulting in weak dependence on M/R . As a result, a given class I pulse profile can be reproduced by a fairly large set of combinations of α , ζ , and M/R . We find that this problem cannot be overcome by deeper observations. Indeed, for simulated deep exposures (~ 1 Ms) with *Constellation-X* the 90% confidence limits alone encompass the entire range of plausible NS radii (7–16 km for an assumed $1.4 M_{\odot}$). Therefore, this class of pulse profiles are not suitable for tight constraints on M/R .

Pulse profiles that occupy region II in Figure 3 exhibit a single broad pulse per rotation. In this configuration, the primary hot spot is observable at all times, while the secondary is visible for only a portion of the spin period. The thermal X-ray pulse profile of PSR J0437–4715 (Zavlin et al. 2002; Zavlin 2006) appears to be in this class. Figure 4 shows simulated observations of PSR J0437–4715, assuming $R = 12$ km and $M = 1.4 M_{\odot}$, with *Constellation-X* XMS and the corresponding best-fit confidence intervals for R . It is apparent that with a substantial improvement in photon statistics, R could, in principle, be constrained to better than 10%, and potentially down to $\sim 2\%$ – 3% (at 90% confidence), given sufficient exposure time. Similar constraints are obtained for $R = 10$ km and $M = 1.4 M_{\odot}$ as well. Combined with an independent mass measurement from radio-timing observations, this method could lead to unprecedented constraints on the NS EOS.

Thermal X-ray light curves that are found in region III (Fig. 2) are characterized by two pulse peaks per rotation period. The nearby PSR J0030+0451 is a good example of this class (Becker et al. 2000; Becker & Aschenbach 2002; see also § 3.1). An advantage of these pulse profiles is that each of the hot spots provides a dominant contribution to the flux of one of the two pulses. This feature has several practical consequences. First, it may, in principle, allow one to determine whether the two polar caps are

² See <http://constellation.gsfc.nasa.gov>.

³ Note that these are defined for the antipodal hot-spot case, but the regions are similar for offset hot spots for small displacements.

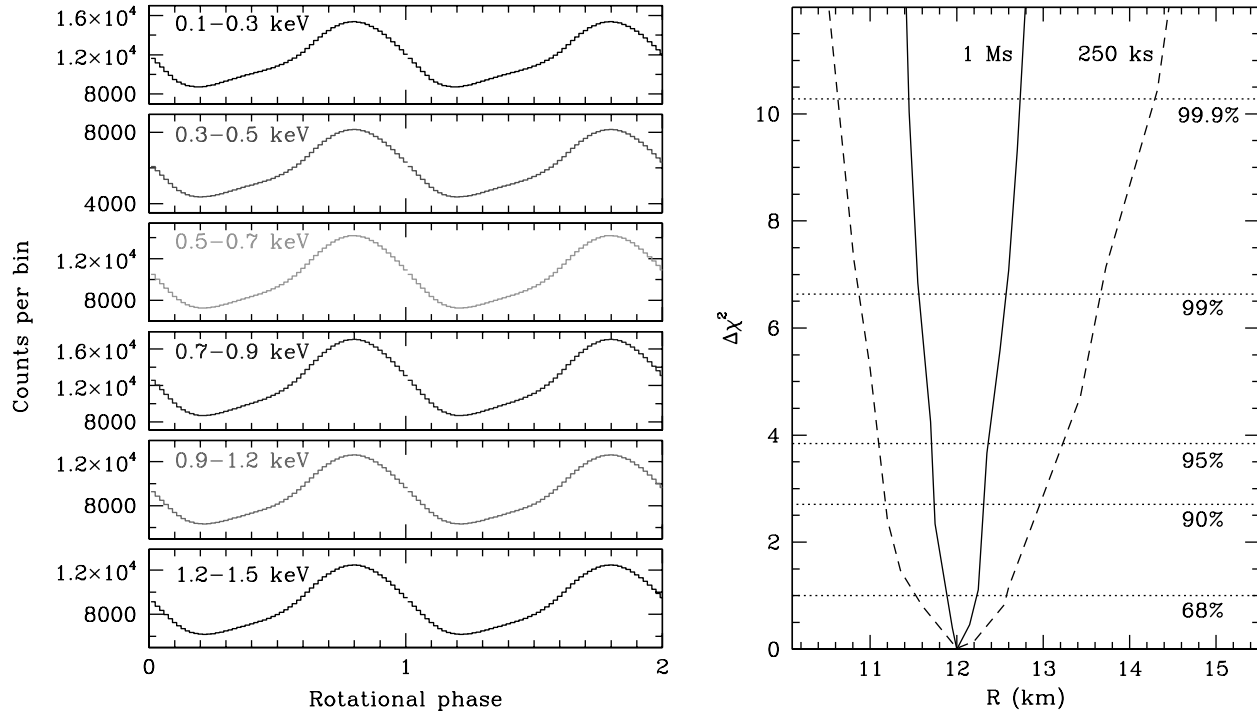


FIG. 4.—*Left*: Simulated 1 Ms spectroscopic and timing observation of PSR J0437–4715 with *Constellation-X* XMS, assuming $R = 12$ km and $M = 1.4 M_{\odot}$. The choice of phase zero is arbitrary. *Right*: Best-fit confidence intervals for R (assuming $M = 1.4 M_{\odot}$) from pulse profile fits to simulated 250 ks and 1 Ms *Constellation-X* XMS observations of PSR J0437–4715. [See the electronic edition of the *Journal* for a color version of this figure.]

identical in terms of size and temperature. Any significant differences would point to deviations from a centered dipole, such as displacements of the dipole along the axial (magnetic north-south) direction or small-scale multipole contributions. Moreover, the sharpness of the two pulses is strongly affected by M/R (see Fig. 3 of Bogdanov et al. 2007), resulting in increased sensitivity to the stellar compactness. Thus, class III appears to be favorable for tight constraints on M/R . We find that a 1 Ms simulated *Constellation-X* observation of PSR J0030+0451 permits constraints on M/R down to a $\sim 5\%$ level (at 90% confidence).

Finally, class IV profiles are formed when both hot spots are observable at all times. As evident in Figure 1, these pulse profiles tend to have significantly lower fluxes relative to classes I–III, since the hot spots are observed close to edge-on for the entire spin period. These pulsars may not be observable at radio wavelengths, due to the large impact angle $|\alpha - \zeta|$, which may exceed the opening half-angle of the radio emission cone. Such an object can be detected only in X-rays. At present, identifying such objects as MSPs through X-ray timing is difficult without a known radio counterpart, although this may be possible with future X-ray observatories (see § 4.1). These factors make class IV MSPs the most difficult to study observationally. Most importantly, as seen in Figure 2, these light curves are much more sensitive to the size and shape of the hot spots. This introduces much larger uncertainties (roughly an order of magnitude greater) than for classes I–III into the spectral and light-curve fits, resulting in weaker constraints on M/R .

Thus, class II and III pulse profile seem to be most favorable for tight constraints on M/R . Fortunately, these two classes occupy a major portion of the α - ζ plane⁴ for the plausible range of M/R , implying that most MSPs should fall into these classes. In Bogdanov et al. (2007), we conducted a detailed study of PSR

J0437–4715, a class II MSP. In § 3, we focus our analysis on two MSPs that exhibit class III pulse profiles.

3. APPLICATION

As seen in § 2, for favorable geometries stringent constraints on MSP parameters are possible. This suggests that even with fairly limited photon statistics, some useful insight into the MSP properties can be obtained. Below, we illustrate this by applying our model to X-ray observations of two nearby MSPs, PSRs J0030+0451 and J2124–3358. Along with J0437–4715, these are the only thermal MSPs for which the X-ray pulse profiles are of sufficient quality to allow meaningful constraints on NS parameters, especially M/R . The spectral analysis for each MSP was performed in XSPEC⁵ version 12.3.0, using the model described above. As shown in Pavlov & Zavlin (1997), Zavlin & Pavlov (1998), and Bogdanov et al. (2007), even the phase-integrated spectra of MSPs are significantly affected by the choice of α and ζ , due to the energy-dependent limb-darkening of the atmosphere, so it is necessary to consider them in the spectral fits as well. In order to apply the model to the X-ray pulse profiles, it was first convolved with the appropriate instrument response, the encircled energy fraction was taken into account, and the sky and detector background were added. The fit was performed by searching the χ^2 hyperspace for the minimum. We fit the pulse profiles by considering the following parameters: the two temperatures and effective radii of each hot spot (T_1 , T_2 , R_1 , and R_2), the two angles α and ζ , the stellar radius R , and the offsets of the secondary hot spot from the antipodal position ($\Delta\alpha$ and $\Delta\phi$). We keep the hydrogen column density along the line of sight (N_H) fixed. Unless noted otherwise, in our analysis we assume a mass of $M = 1.4 M_{\odot}$ and allow R to vary within the range of plausible NS radii for this mass (7–15 km; see, e.g., Lattimer & Prakash 2001).

⁴ The same holds true in the $\cos\alpha$ - $\cos\zeta$ space.

⁵ See <http://heasarc.gsfc.nasa.gov/docs/xanadu/xspec>.

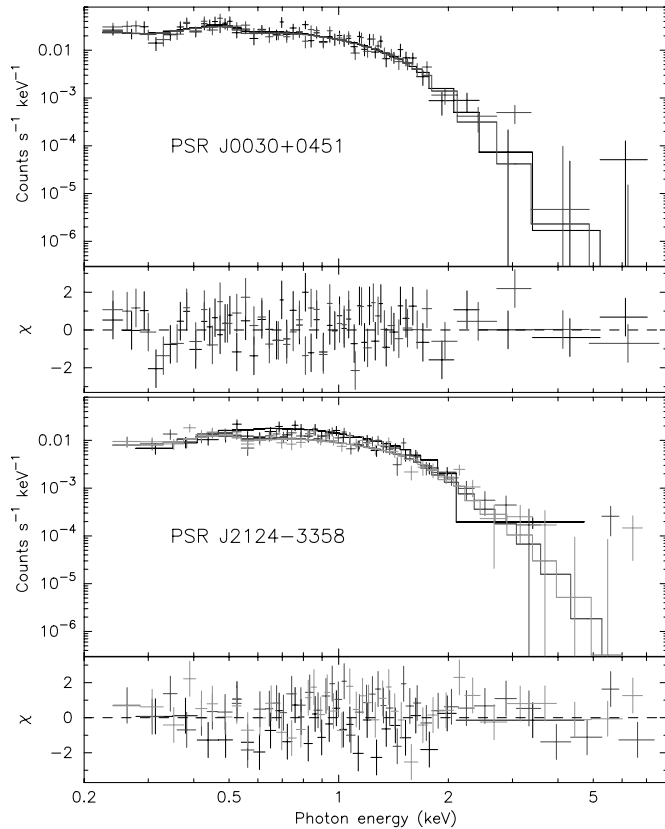


FIG. 5.—*Top:* *XMM-Newton* EPIC MOS1/2 phase-integrated spectra of J0030+0451 fitted with a two-temperature hydrogen atmosphere thermal model. The lower part shows the best-fit residuals. *Bottom:* *Chandra* ACIS-S and *XMM-Newton* EPIC MOS1/2 phase-integrated spectra of PSR J2124–3358 fitted with a two-temperature hydrogen atmosphere model. [See the electronic edition of the *Journal* for a color version of this figure.]

3.1. PSR J0030+0451

This 4.86 ms solitary pulsar was discovered at radio wavelengths in the Arecibo drift scan survey (Lommen et al. 2000). It was subsequently detected with *Röntgensatellit* (*ROSAT*) during the final days of this mission. Due to the unstable behavior of the failing PSPC detector, these data provided no reliable spectral information, but revealed a double-peaked pulse profile with a pulsed fraction $\sim 50\%$ (Becker et al. 2000). PSR J0030+0451 was revisited in 2001 June 19 by *XMM-Newton* for 31 ks (Becker & Aschenbach 2002). This observation revealed a 0.3–2 keV spectrum qualitatively similar to that of J0437–4715. In addition, the EPIC pn X-ray pulse profile shows a relatively high pulsed fraction ($\sim 50\%$ for 0.3–2 keV) with two prominent pulses. Lommen et al. (2000) have estimated from radio polarization measurements two possible pulsar geometries, $\alpha = 8^\circ$ and $\beta = 1^\circ$, or $\alpha = 62^\circ$ and $\beta = 10^\circ$, where β is the angular separation of the line of sight with respect to the magnetic axis at closest approach. As the former combination of angles cannot produce the observed double-peaked X-ray profile for all plausible choices of M/R (see Figs. 1 and 3), even if we allow for substantial offsets of the secondary hot spots in α and ϕ , $\alpha = 8^\circ$, $\beta = 1^\circ$ can be definitively ruled out. This result implies that the observed radio interpulse (Lommen et al. 2000) most likely originates from the antipodal radio emission cone, not from the same emission cone as the main pulse.

Figure 5 shows the *XMM-Newton* EPIC MOS1/2 spectra of PSR J0030+0451. They are well described by two thermal components. Fitting a hydrogen atmosphere model to the spectrum

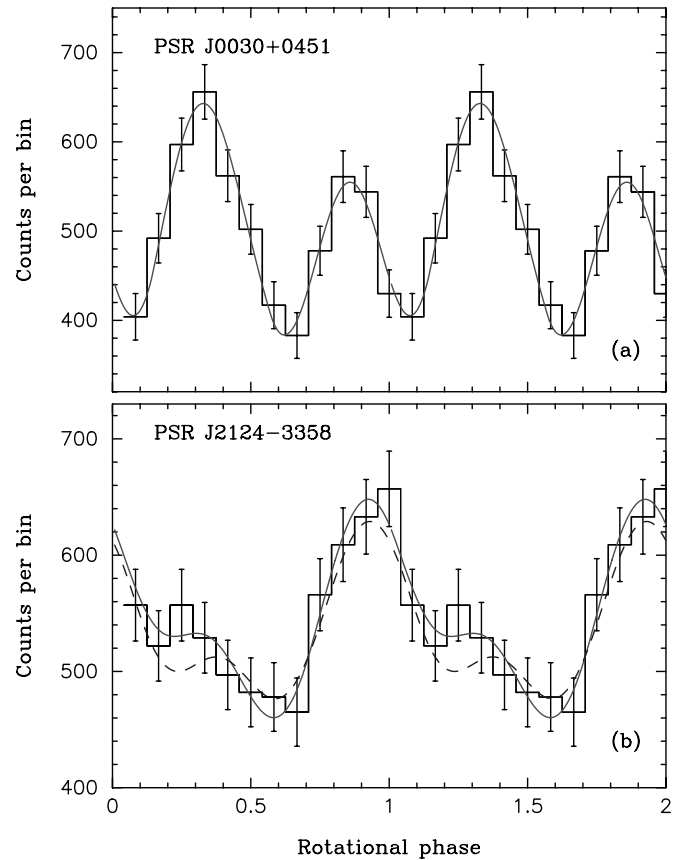


FIG. 6.—(a) *XMM-Newton* EPIC pn pulse profile of PSR J0030+0451 for 0.3–2 keV. The solid line shows the best-fit model. (b) *XMM-Newton* EPIC pn pulse profile of PSR J2124–3358 for 0.3–2 keV. The solid line shows the best-fit model, while the dashed line shows the best fit for a centered dipole (see text for best-fit parameters). [See the electronic edition of the *Journal* for a color version of this figure.]

yields $T_1 = (1.3\text{--}2.1) \times 10^6$ K, $R_1 = 0.01\text{--}0.54$ km, $T_2 = (0.3\text{--}0.7) \times 10^6$ K, $R_2 = 0.8\text{--}3.5$ km, and $F_X = 1.5 \times 10^{-13}$ ergs s $^{-1}$ (0.3–2 keV), for assumed $N_H = (1\text{--}3) \times 10^{20}$ cm $^{-2}$, $M = 1.4 M_\odot$, $R = 7\text{--}15$ km, and all combinations of α and ζ in the range $0^\circ\text{--}90^\circ$. The ranges quoted are 1σ limits. As expected, the spectral continuum is fit equally well with a blackbody model. Becker & Aschenbach (2002) have suggested a broken power law as a possible alternative interpretation of the spectrum of J0030+0451. However, as pointed out by Zavlin (2007), this model results in unrealistic values of N_H and is thus unlikely.

The fit to the pulse profile (Fig. 6a) was carried out by fixing $N_H = 2 \times 10^{20}$ cm $^{-2}$ and taking a distance of $D = 300$ pc (Lommen et al. 2006). For $M = 1.4 M_\odot$, the radius is constrained to be $R > 9.4$ km or, more generally, $R/R_S > 2.3$ (68% confidence) for all combinations of the other free parameters, with a best-fit $\chi^2_\nu = 0.81$ (for 3 degrees of freedom). Acceptable fits were obtained for radii up to ~ 20 km. In the case of a blackbody model, we find that good fits to the X-ray pulse profile require implausibly large stellar radii (≥ 20 km). As no NS EOS models predict radii exceeding ~ 15 km for $M = 1.4 M_\odot$ (see Lattimer & Prakash 2001), the validity of the blackbody interpretation is very doubtful. The lower limit on the allowed values of α and ζ is found to be $\geq 44^\circ$ (68% confidence), obtained when the other angle is equal to 90° . Namely, if $\alpha = 90^\circ$, then $\zeta = 44^\circ$, or if $\alpha = 44^\circ$, then $\zeta = 90^\circ$. Finally, the currently available data are consistent with both a centered and a displaced dipole field.

3.2. PSR J2124–3358

PSR J2124–3358 is a nearby ($D \approx 250$ pc), isolated pulsar with $P = 4.93$ ms (Bailes et al. 1997) first observed in X-rays with the *ROSAT* HRI (Becker & Trümper 1999). As the HRI provided no useful spectral information, only a pulse profile was obtained with pulsed fraction $\sim 33\%$. J2124–3358 was later observed with *Chandra* ACIS-S for 30.2 ks and with *XMM-Newton* EPIC MOS1/2 and EPIC pn for 68.9 and 66.8 ks, respectively (Zavlin 2006; Hui & Becker 2006). As shown by Zavlin (2006), the X-ray emission from J2124–3358 is also well described by a two-temperature thermal spectrum. Fitting our hydrogen atmosphere model to the phase-integrated spectral continuum yields $T_1 = (1.3\text{--}2.4) \times 10^6$ K, $R_1 = 0.03\text{--}0.5$ km, $T_2 = (0.3\text{--}0.8) \times 10^6$ K, $R_2 = 0.9\text{--}3.1$ km, and $L_X = 1.8 \times 10^{30}$ ergs s $^{-1}$ (0.3–2 keV), for assumed $D = 250$ pc, $N_H = 1 \times 10^{20}$ cm $^{-2}$, $M = 1.4 M_\odot$, $\alpha = 0^\circ\text{--}90^\circ$, $\zeta = 0^\circ\text{--}90^\circ$, and $R = 7\text{--}15$ km. The uncertainties quoted represent $\pm 1 \sigma$ ranges. The derived values are consistent with the results obtained by Zavlin (2006). Note that the diffuse X-ray emission detected around this MSP (Hui & Becker 2006) does not contribute appreciably to the point-source MSP emission, as its total luminosity $L_X \sim 1 \times 10^{29}$ ergs s $^{-1}$ (0.1–2.4 keV) is negligible.

The X-ray pulse profile of this MSP (Fig. 6b) exhibits marginal evidence for a faint secondary peak. Given that this feature is evident in both the *ROSAT* PSPC (Becker & Trümper 1999) and *XMM-Newton* EPIC pn (Zavlin 2006) pulse profile, it is very likely genuine. The fit to the pulse profile (Fig. 6b) was carried out by fixing $N_H = 1 \times 10^{20}$ cm $^{-2}$ (Zavlin 2006) and assuming the dispersion measure–derived distance of $D = 250$ pc. Assuming $M = 1.4 M_\odot$, the radius is constrained to be $R > 7.8$ km (68% confidence), with best fit $\chi^2_\nu = 1.20$ (for 3 degrees of freedom). The angles α and ζ are constrained to be $\geq 12^\circ$ (68% confidence) for the other angle equal to 90° (i.e., if $\alpha = 90^\circ$, then $\zeta = 12^\circ$, or if $\alpha = 12^\circ$, then $\zeta = 90^\circ$). Although the suggestive asymmetry of the pulse profile hints at the presence of an offset dipole, the poor photon statistics permit a centered dipole configuration. As with PSR J0030+0451, a blackbody model requires unrealistically large stellar radii ($\gtrsim 20$ km for $M = 1.4 M_\odot$) for J2124–3358. Thus, we conclude that a blackbody model does not provide a valid description of the surface emission properties of PSR J2124–3358 as well.

4. DISCUSSION

4.1. Searches for Radio-Quiet MSPs

The effect of light bending, combined with the (nearly) antipodal configuration of the two MSP hot spots, ensures that the thermal radiation is observable at Earth for any combination of α and ζ . In contrast, at radio frequencies a pulsar is not observable if $|\alpha - \zeta|$ exceeds the opening half-angle ρ of the radio emission cone. This brings out the intriguing prospect of detecting and identifying such radio-quiet MSPs in X-rays using blind pulsation searches. With the currently available X-ray observatories (*Chandra* and *XMM-Newton*), this endeavor is rather difficult, due to the intrinsic faintness of MSPs (see, e.g., Cameron et al. 2007) and their relatively low X-ray–pulsed fractions ($\lesssim 50\%$). On the other hand, for the next generation of large X-ray observatories (*Constellation-X* and *XEUS*), the proposed $\gtrsim 10$ -fold increase in sensitivity makes such a survey quite feasible.

Figure 7 shows the X-ray–pulsed fraction of a $1.4 M_\odot$ MSP with a 10, 12, and 14 km radius as a function of α and ζ , assuming a thermal emission spectrum like that of PSR J0437–4715 (Zavlin 2006; Bogdanov et al. 2007). Also shown are lines delineating the region of the α – ζ plane for which a pulsar with a

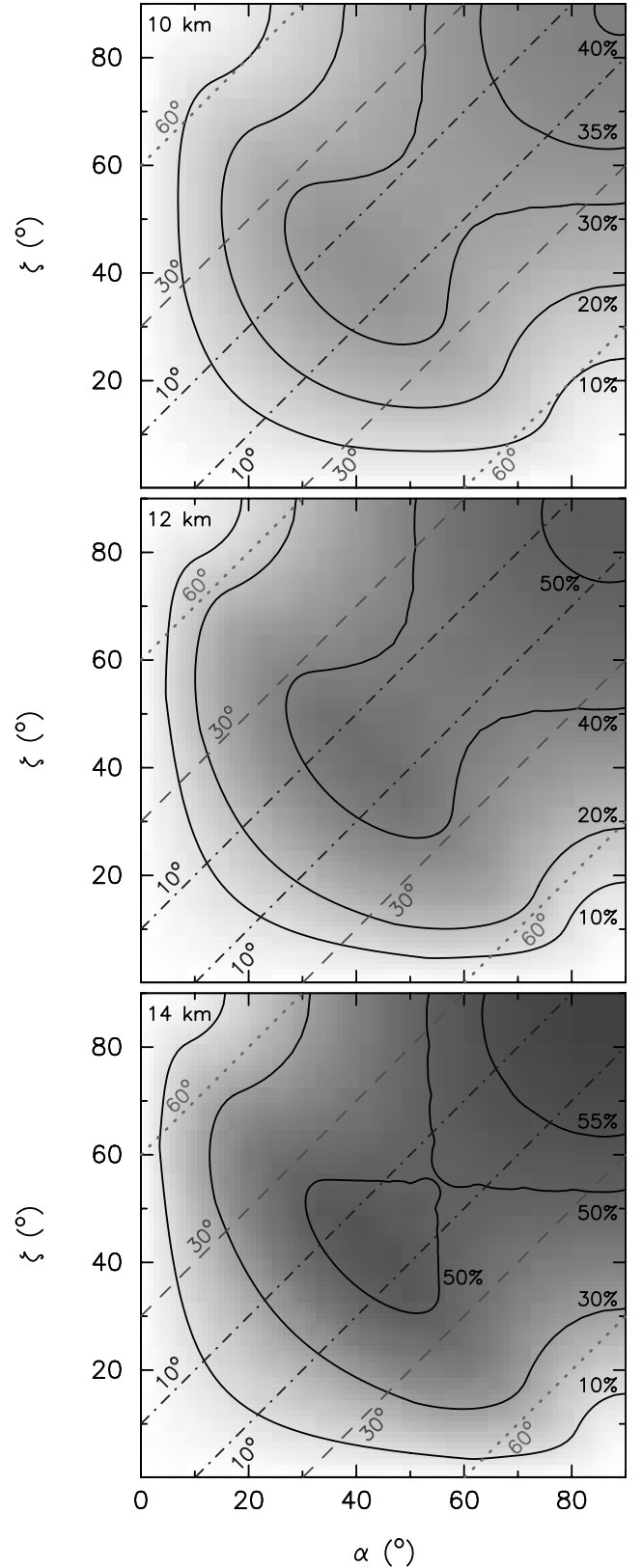


FIG. 7.—Contours of constant pulsed fraction (solid lines) for X-ray H atmosphere emission from two antipodal hot spots in the 0.3–2 keV band as a function of the pulsar obliquity (α) and viewing angle (ζ) for a $1.4 M_\odot$ MSP with radius 10, 12, and 14 km (from top to bottom, respectively). The X-ray emission spectrum is taken to be that of PSR J0437–4715. The diagonal dot-dashed line, dashed line, and dotted lines show 10° , 30° , and 60° opening half-angles of the radio emission cone, respectively. All MSPs found between each pair of lines are detectable at radio frequencies (see text for details). [See the electronic edition of the Journal for a color version of this figure.]

given radio emission cone width is observable at radio frequencies. Note that the true opening angle of the radio cone for a given MSP is not known and is difficult to measure reliably, but could be as high as $\sim 60^\circ$ (see Kramer et al. 1998). If we assume a uniform distribution of pulsar obliquities (α) and viewing angles (ζ), for $\rho \lesssim 30^\circ$ a substantial portion ($\sim 45\%$) of the MSP population is invisible to us in the radio. On the other hand, if we consider an X-ray–timing survey with a limiting pulsed fraction sensitivity of $\sim 10\%$, only $\sim 5\%$ – 20% (depending on M/R) of the MSPs will go undetected as pulsed sources, although they will still be detected as X-ray sources (provided they are not heavily absorbed). The Galactic population of MSPs may in fact be preferentially clustered in a certain range of α , due to the poorly understood effects of the accretion and magnetic field reduction processes during the LMXB phase on the NS (see, e.g., Bhattacharya & van den Heuvel [1991] for a review). A deep X-ray–timing survey of nearby ($\lesssim 2$ kpc) MSPs may, in principle, reveal whether this is indeed the case.

The detectability of the thermal polar cap emission from MSPs for all combinations of α and ζ further suggests that the *entire* MSP population of certain Galactic globular clusters (e.g., 47 Tuc; see Grindlay et al. 2002; Bogdanov et al. 2006a; Cameron et al. 2007) could be detected using high angular and temporal resolution X-ray imaging and timing (e.g., with the aid of the proposed *Generation-X* observatory). Identifying the whole population of MSPs in a cluster has important implication for studies of globular cluster evolution and internal dynamics (see, e.g., Camilo & Rasio 2005 and references therein).

4.2. Constraining Magnetic Field Evolution Models

As shown in Bogdanov et al. (2007) and in this present paper, the morphology of the thermal X-ray pulse profiles of MSPs offers useful insight into the magnetic field geometry of the pulsar (Fig. 1). This has important implications for pulsar magnetic field evolution models. For instance, Ruderman (1991; see also Chen & Ruderman [1993] and Chen et al. [1998]) has postulated the presence of crustal “plates” on the NS surface formed by shear stresses on the crust caused by neutron superfluid vortex lines pinned to lattice nuclei (see Fig. 3 of Chen et al. 1998). The motion of these plates would cause the magnetic fields of MSPs to migrate across the stellar surface, resulting in either an aligned magnetic field or one “pinched” at the spin pole. However, these configurations would result in very little (\lesssim a few percent) modulation of the thermal X-ray flux, due to the close alignment of the polar caps with the spin axis, regardless of the viewing geometry. This is at odds with the observed thermal X-ray–pulsed fractions of PSRs J0437–4715, J0030+0451, and J2124–3358, which are in the range 30%–50%. Thus, although the model of Ruderman (1991) can reproduce the observed radio properties of MSPs, it is inconsistent with the observed thermal X-ray pulse profiles of MSPs. In particular, the X-ray pulse profiles of PSRs J0437–4715, J0030+0451, and J2124–3358 indicate that the magnetic axes of these MSPs are significantly misaligned from the spin axis. This, in turn, implies that the dipole fields of these

(and likely all) MSPs do not have a tendency to align with the spin axis or migrate toward one of the spin poles.

5. CONCLUSIONS

We have examined the properties of our model of thermal emission from hot spots on the surface of a neutron star covered by a hydrogen atmosphere, relevant for MSPs. Our investigation has demonstrated that energy-resolved modeling of the thermal X-ray pulse profiles and phase-resolved spectroscopy of the continuum emission can, in principle, be used to determine M/R and the pulsar geometry to high accuracy, given observational data of sufficient quality and favorable values of α and ζ . As shown in § 2.1, the thermal pulse profiles are surprisingly insensitive to the details of the polar cap size and shape, the distance to the pulsar, and the uncertainty in the instrument effective area. This method represents the only feasible approach of studying the MSP magnetic field, surface properties, and compactness, especially for isolated MSPs. Barring any deleterious effect, such as additional hidden spectral components (see, e.g., Bogdanov et al. 2006b and references therein), this approach can, in principle, lead to unprecedented insight into NS properties.

Our model is found to agree with the observed emission from the nearby solitary MSPs J0030+0451, and J2124–3358. As with PSR J0437–4715 (Bogdanov et al. 2007), the relatively large pulsed fractions observed in PSRs J0030+0451 and J2124–3358 require the existence of a light-element atmosphere on the stellar surface and cannot be reproduced by a blackbody model for realistic NS radii. For J0030+0451 and J2124–3358, we are able to place interesting limits on the allowed compactness of $R > 9.4$ km and $R > 7.8$ km (68% confidence), assuming $M = 1.4 M_\odot$. Based on our findings in § 2, we expect deeper observations of this MSP to lead to much tighter constraints on M/R , which in turn may firmly rule out certain families of NS EOS. The available thermal X-ray pulse profiles also provide useful constraints on magnetic field models of MSPs. Specifically, the positions of the magnetic polar caps on the NS surface implied by the X-ray data indicate that the magnetic field closely resembles the conventional oblique dipole model of pulsars, rather than more exotic field configurations.

The success of this approach toward elucidating crucial NS properties motivates further studies of the nearby sample of MSPs with both *Chandra* and *XMM-Newton*. Moreover, this makes MSPs particularly important targets for upcoming X-ray missions such as *Constellation-X* and *XEUS*. The great increase in throughput of these facilities will allow searches for new MSPs, detailed observations of a larger sample of known radio MSPs, and unprecedented constraints on key NS properties, especially the NS EOS.

We would like to thank Ramesh Narayan, Bryan Gaensler, Deepto Chakrabarty, Pat Slane, and Alice Harding for numerous useful suggestions. This work was funded in part by NASA *Chandra* grant G07-8033A. The research presented has made use of the NASA Astrophysics Data System (ADS).

REFERENCES

- Bailes, M., et al. 1997, *ApJ*, 481, 386
- Becker, W., & Aschenbach, B. 2002, in *Proceedings of the 270. WE-Heraeus Seminar on Neutron Stars, Pulsars, and Supernova Remnants*, ed. W. Becker, H. Lech, & J. Trümper (Garching: MPE)
- Becker, W., & Trümper, J. 1999, *A&A*, 341, 803
- Becker, W., Trümper, J., Lommen, A. N., & Backer, D. C. 2000, *ApJ*, 545, 1015
- Beloborodov, A. M. 2002, *ApJ*, 566, L85
- Bhattacharya, D., & van den Heuvel, E. P. J. 1991, *Phys. Rep.* 203, 1
- Biggs, J. D. 1990, *MNRAS*, 245, 514
- Bogdanov, S., Grindlay, J. E., Heinke, C. O., Camilo, F., Freire, P. C. C., & Becker, W. 2006a, *ApJ*, 646, 1104
- Bogdanov, S., Grindlay, J. E., & Rybicki, G. B. 2006b, *ApJ*, 648, L55
- Bogdanov, S., Rybicki, G. B., & Grindlay, J. E. 2007, *ApJ*, 670, 668
- Cadeau, C., Morsink, S. M., Leahy, D., & Campbell, S. S. 2007, *ApJ*, 654, 458
- Cameron, P. B., Rutledge, R. E., Camilo, F., Bildsten, L., Ransom, S. M., & Kulkarni, S. R. 2007, *ApJ*, 660, 587

- Camilo, F., & Rasio, F. A. 2005, in ASP Conf. Ser. 328, Binary Radio Pulsars, ed. F. A. Rasio & I. H. Stairs (San Francisco: ASP), 147
- Chen, K., & Ruderman, M. S. 1993, *ApJ*, 408, 179
- Chen, K., Ruderman, M., & Zhu, T. 1998, *ApJ*, 493, 397
- Grindlay, J. E., Camilo, F., Heinke, C. O., Edmonds, P. D., Cohn, H., & Lugger, P. 2002, *ApJ*, 581, 470
- Harding, A. K., & Muslimov, A. G. 2002, *ApJ*, 568, 862
- Hui, C. Y., & Becker, W. 2006, *A&A*, 448, L13
- Kramer, A., Xilouris, K. M., Lorimer, D. R., Doroshenko, O., Jessner, A., Wielebinski, R., Wolszczan, A., & Camilo, F. 1998, *ApJ*, 501, 270
- Lattimer, J. M., & Prakash, M. 2001, *ApJ*, 550, 426
- Lommen, A. N., Kipphorn, R. A., Nice, D. J., Splaver, E. M., Stairs, I. H., & Backer, D. C. 2006, *ApJ*, 642, 1012
- Lommen, A. N., Zepka, A., Backer, D. C., McLaughlin, M., Cordes, J. M., Arzoumanian, Z., & Xilouris, K. 2000, *ApJ*, 545, 1007
- McClintock, J. E., Narayan, R., & Rybicki, G. B. 2004, *ApJ*, 615, 402
- Narayan, R., & Vivekanand, M. 1983, *A&A*, 122, 45
- Pavlov, G. G., & Zavlin, V. E. 1997, *ApJ*, 490, L91
- Ruderman, M. 1991, *ApJ*, 366, 261
- Zavlin, V. E. 2006, *ApJ*, 638, 951
- . 2007, *Ap&SS*, 308, 297
- Zavlin, V. E., & Pavlov, G. G. 1998, *A&A*, 329, 583
- Zavlin, V. E., Pavlov, G. G., Sanwal, D., Manchester, R. N., Trümper, J., Halpern, J. P., & Becker, W. 2002, *ApJ*, 569, 894
- Zavlin, V. E., Pavlov, G. G., & Shibano, Yu. A. 1996, *A&A*, 315, 141
- Zhang, L., & Cheng, K. S. 2003, *A&A*, 398, 639